

## Variable dual-frequency electrostatic wave launcher for plasma applications

Benjamin Jorns, Robert Sorenson, and Edgar Choueiri

Citation: [Review of Scientific Instruments](#) **82**, 123501 (2011); doi: 10.1063/1.3664785

View online: <http://dx.doi.org/10.1063/1.3664785>

View Table of Contents: <http://scitation.aip.org/content/aip/journal/rsi/82/12?ver=pdfcov>

Published by the [AIP Publishing](#)

---

### Articles you may be interested in

[Wide-bandwidth charge sensitivity with a radio-frequency field-effect transistor](#)

Appl. Phys. Lett. **103**, 143102 (2013); 10.1063/1.4822430

[Inclined slot-excited annular electron cyclotron resonance plasma source for hyperthermal neutral beam generation](#)

Rev. Sci. Instrum. **82**, 013502 (2011); 10.1063/1.3523425

[Reduction of the electrostatic coupling in a large-area internal inductively coupled plasma source using a multicusp magnetic field](#)

Appl. Phys. Lett. **85**, 1677 (2004); 10.1063/1.1784877

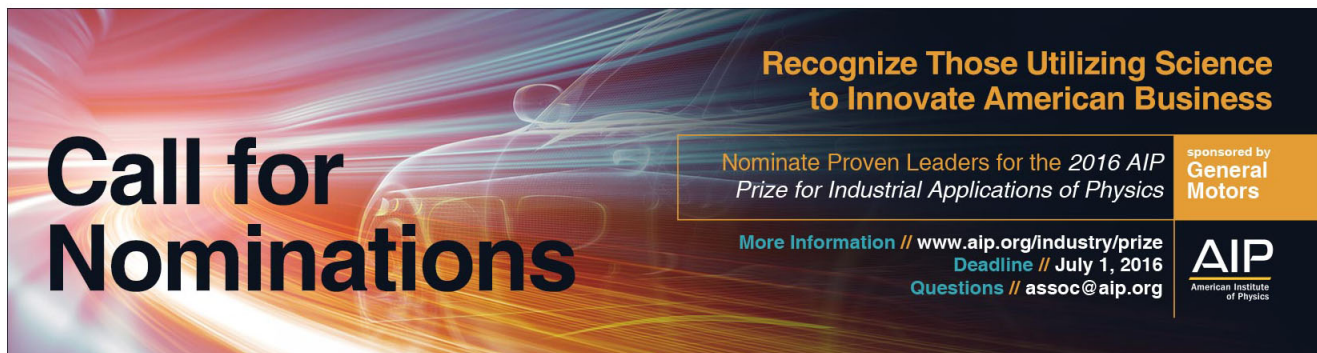
[Transitions from electrostatic to electromagnetic whistler wave excitation](#)

Phys. Plasmas **11**, 2144 (2004); 10.1063/1.1689352

[Spectral and spatial characterization of a radio frequency power absorption in high pressure helicon plasmas](#)

Phys. Plasmas **8**, 4659 (2001); 10.1063/1.1394779

---



**Call for Nominations**

**Recognize Those Utilizing Science to Innovate American Business**

Nominate Proven Leaders for the *2016 AIP Prize for Industrial Applications of Physics*

More Information // [www.aip.org/industry/prize](http://www.aip.org/industry/prize)  
Deadline // July 1, 2016  
Questions // [assoc@aip.org](mailto:assoc@aip.org)

sponsored by  
**General Motors**

**AIP**  
American Institute of Physics

## Variable dual-frequency electrostatic wave launcher for plasma applications

Benjamin Jorns, Robert Sorenson, and Edgar Choueiri

*Electric Propulsion and Plasma Dynamics Laboratory, Mechanical and Aerospace Engineering,  
Princeton University, Princeton, New Jersey 08544, USA*

(Received 6 June 2011; accepted 6 November 2011; published online 7 December 2011)

A variable tuning system is presented for launching two electrostatic waves concurrently in a magnetized plasma. The purpose of this system is to satisfy the wave launching requirements for plasma applications where maximal power must be coupled into two carefully tuned electrostatic waves while minimizing erosion to the launching antenna. Two parallel LC traps with fixed inductors and variable capacitors are used to provide an impedance match between a two-wave source and a loop antenna placed outside the plasma. Equivalent circuit analysis is then employed to derive an analytical expression for the normalized, average magnetic flux density produced by the antenna in this system as a function of capacitance and frequency. It is found with this metric that the wave launcher can couple to electrostatic modes at two variable frequencies concurrently while attenuating noise from the source signal at undesired frequencies. An example based on an experiment for plasma heating with two electrostatic waves is used to demonstrate a procedure for tailoring the wave launcher to accommodate the frequency range and flux densities of a specific two-wave application. This example is also used to illustrate a method based on averaging over wave frequencies for evaluating the overall efficacy of the system. The wave launcher is shown to be particularly effective for the illustrative example—generating magnetic flux densities in excess of 50% of the ideal case at two variable frequencies concurrently—with a high adaptability to a number of plasma dynamics and heating applications. © 2011 American Institute of Physics. [doi:10.1063/1.3664785]

### I. INTRODUCTION

A number of industrial and research related applications depend on the efficient coupling of electrostatic (ES) waves to a magnetized plasma. In many of these processes, a single ES wave is sufficient to drive the application; however, for some significant experimental studies in basic plasma dynamics, plasma heating, and plasma propulsion, two ES waves are necessary to achieve the desired effect. For example, in a study of ion dynamics, it has been proposed that the non-linear interaction of two ES waves may explain anomalous ion acceleration that has been observed in the earth's ionosphere.<sup>1</sup> In order to experimentally confirm this, it is necessary to construct a closed terrestrial configuration in which the ES wave parameters—primarily the wave frequencies  $f_1$  and  $f_2$ —can be carefully tuned to simulate the ionospheric conditions.

In terms of applications that depend on two-wave processes for plasma heating, it has been found that two ES waves propagating in the direction perpendicular to a uniform magnetic field will produce non-resonant acceleration when  $f_2 - f_1 = nf_{ci}$ , where  $n$  is an integer number, and  $f_{ci}$  is the ion cyclotron frequency.<sup>2-5</sup> This process is characterized by the ability to efficiently heat initially thermalized plasmas<sup>6</sup> for applications such as closed fusion experiments and industrial processes. As with the case of ion acceleration in the ionosphere, any experimental characterization of this mechanism requires a setup in which the waves can be launched effectively and carefully controlled.

Finally, with respect to plasma propulsion applications, it has been proposed that the non-resonant nature of a two ES wave interaction may be adapted for use in a thruster.<sup>7</sup> In this case, the two waves are adjusted in order to provide

a strong driving mechanism for directed ion acceleration in a magnetized plasma.

These examples serve to illustrate a few of the important applications that can be achieved with two ES waves. However, as the success of these processes depends on the ability to couple and control two ES waves in a magnetized plasma, it is apparent that any experimental investigation or physical application must be designed with a specialized wave-launching system in mind—one that will (I) maximize power into two waves simultaneously at the variable frequencies  $f_1$ ,  $f_2$  and (II) attenuate any undesired frequencies not equal to  $f_1$  and  $f_2$ . These criteria ensure that only the waves of interest are excited in the plasma while harmonic distortions that may arise from a non-ideal generating source are blocked. Additionally, for many applications—primarily plasma heating and space propulsion—it is necessary to reduce component weight as well as minimize the material erosion that can result from exposure of the antenna to the plasma. As a consequence, we further impose the condition that the wave system must operate externally to the plasma and with only a single power source.

The goal of this paper is to present a variable dual-frequency wave launcher (VDWL) that satisfies the above criteria. In the first section, we outline the system including the choice of antenna and matching network for the desired applications. In the second section, we validate our technique and its performance in satisfying I and II with the illustrative example of the beating waves experiment II (BWX II) whose goal is to investigate the second application outlined above. In the final section, we discuss the insights gained from the VDWL employed in BWX II and a procedure for how to

design VDWLs to accommodate applications with higher powers and frequency ranges outside the scope of this illustrative example.

## II. VARIABLE DUAL-FREQUENCY WAVE LAUNCHER

The VDWL we present is designed to operate with experiments where an antenna placed around the plasma volume serves to excite the ES waves. One example of such a setup that is common to most of the applications described in the previous section is a cylindrically bounded plasma with an axial magnetic field. The VDWL for this system and similar geometries is characterized by two important components: the inductive antenna and a dual-frequency matching network.

### A. Inductive antenna

While a number of studies have indicated electrostatic waves can be generated efficiently in a magnetized plasma by capacitive plates,<sup>8</sup> capacitively coupled concentric rings,<sup>9</sup> planar antenna,<sup>10,11</sup> and current-carrying wires along the axis of the plasma,<sup>12,13</sup> all of these methods subject the antenna to significant erosion. Since potential applications of the two-wave process depend on maintaining component integrity, the VDWL employs a loop antenna placed outside the plasma for launching the electrostatic waves. In this configuration, the antenna generates a time-varying magnetic flux in the direction perpendicular to the ambient magnetic field. This in turn induces a substantial charge gradient in the plasma, which couples to both perpendicular and oblique electrostatic waves. The type of wave that is excited depends on the geometry of the inductive antenna. Two commonly employed configurations include the Nagoya III for coupling to the electric field component of helicon modes in a magnetized plasma<sup>14</sup> and a Helmholtz coil antenna that excites the electrostatic ion cyclotron wave.<sup>15</sup> In both cases, the strength of the coupling depends on the magnetic flux through the plasma volume, which is a function of the antenna inductance. We model this inductance with an equivalent circuit for the antenna that consists of a series resistor,  $R_A$ , and inductor,  $L_A$ , in parallel with a parasitic capacitor,  $C_A$ .

### B. Dual frequency matching network

As the wave coupling for the inductive antenna depends directly on the average magnetic flux density, the criteria outlined in Secs. I and II for our wave launching system are now framed in the context of this physical parameter. Specifically, we need a matching network for the antenna that is capable of maximizing the magnetic flux density for two variable frequencies while simultaneously attenuating the flux at frequencies other than the selected values,  $f_1, f_2$ . We note here that while this selectivity is necessary to block undesirable harmonic distortions from the wave source, this latter feature also has added value for experiments in which the plasma is initially created by radio frequency waves. The noise from such a process can induce voltage fluctuations on the heating antenna that unattenuated could produce harmful feedback into the signal amplifier.

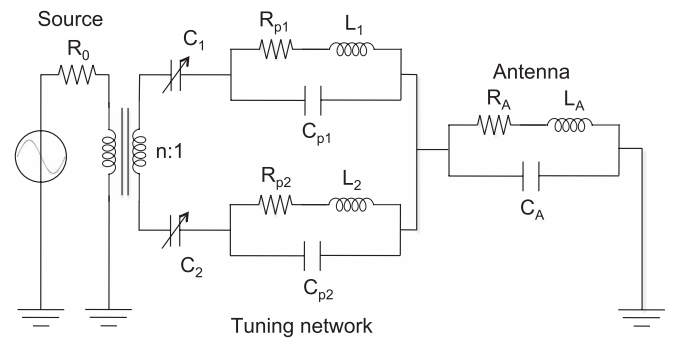


FIG. 1. Dual frequency tuning circuit with equivalent circuit models for each component. The transformer has an  $n:1$  turns ratio.

The magnetic flux density for these loop antennae depends linearly on the the current they admit. This leads to an expression for the the average flux density in the plasma volume,

$$\langle B \rangle = \alpha N I_A, \quad (1)$$

where  $N$  is the number of turns in the antenna,  $I_A$  is the current per turn, and  $\alpha$  is a fixed constant that depends on the geometry. Since the number of turns and geometry of the heating antenna are typically constrained by the availability of space and the type of excited mode that is desired, the antenna current is the free parameter we manipulate to achieve the performance goals cited above. This is accomplished with the dual frequency network shown in Fig. 1 along with the equivalent circuit for the loop antenna.

The tuning network consists of an  $n:1$  step-down transformer between the source with impedance  $R_0$  and two parallel LC traps connected in series with the antenna. The parasitic components ( $C_{p1}, R_{p1}, C_{p2}, R_{p2}$ ) account for the non-ideal behavior of the inductors. During operation, the LC traps provide two separate and isolated paths for the waves from the source's combined signal. As a result, only one frequency  $f_1$  is passed through the top arm, while the second frequency  $f_2$  is passed through the bottom arm. By tuning the series resonance of the inductors  $L_1, L_2$  and the variable capacitors  $C_1, C_2$ , not only can the values of  $f_1, f_2$  be changed, but the circuit will provide a conjugate match to the load at these values. The step down transformer serves to match the residual resistance to the source impedance, which in turn multiplies the current through the antenna at the tuned frequencies. In this way, the circuit is capable of selectively passing two frequencies concurrently and attenuating the surrounding frequency spectrum.

We can quantify the performance of this system with an expression for the current through the antenna. For a fixed voltage  $V_S$  at the source, the current through  $L_A$  is given by

$$I_A = nV_S \left| \frac{Z_A}{(R_A + j\omega L_A)(R_0 + n^2[Z_T + Z_A])} \right|, \quad (2)$$

where  $\omega$  is the angular frequency and the factors of  $n$  and  $n^2$  stem from the transformer.  $Z_T$  is the impedance of the tuning

network which is given by

$$Z_T = \left( \sum_{i=1,2} \left[ \left( \frac{1}{R_{pi} + j\omega L_i} + j\omega C_{pi} \right)^{-1} + \frac{1}{j\omega C_i} \right]^{-1} \right)^{-1}. \quad (3)$$

$Z_A$  denotes the impedance of the antenna, which from the equivalent circuit model is

$$Z_A = \left( \frac{1}{R_A + j\omega L_A} + j\omega C_A \right)^{-1}. \quad (4)$$

It is evident from Eq. (2) that the LC traps introduce poles at two frequencies, which we denote  $f_1, f_2$ . Moreover, since these resonant frequencies are functions of the component values, we can use Eq. (2) to calculate numerically the values necessary to produce resonances at arbitrary  $f_1$  and  $f_2$ . While this procedure will yield a wide range of valid component values for isolating  $f_1, f_2$ , we choose to constrain our inductor values such that  $L_1, L_2 \gg L_A$ . We do this for two reasons. First, provided the parasitic resistances  $R_{p1}, R_{p2}$  are sufficiently small, this constraint yields simplified expressions for the resonant frequencies,

$$f_1 \approx \frac{1}{2\pi\sqrt{L_1 C_1}} \quad f_2 \approx \frac{1}{2\pi\sqrt{L_2 C_2}}. \quad (5)$$

This convenient relationship between the tuned frequencies and capacitances gives us a first-order approximation for how to tune our components. The second reason for this restriction on inductance is that the loop antenna typically will have a low inductance. As a consequence, for low frequency applications where  $L_1, L_2 \approx L_A$ , commercially available variable capacitors may not produce sufficient capacitance for the LC traps to function. In order to continue to employ these variable capacitors for effective tuning, we instead are forced to use large inductors  $L_2, L_1 \gg L_A$ . This restriction is relaxed as the frequency range of interest is increased.

With these considerations in mind, we use Eqs. (1) and (2) to find an approximation for the normalized magnetic flux density,  $\beta$ , produced by the antenna as a function of component values and frequency

$$\beta = \frac{\langle B \rangle}{\langle B_0 \rangle} = \left| \frac{2n (R_0 R_A)^{1/2} Z_A}{(R_A + j\omega L_A) (R_0 + n^2 [Z_T + Z_A])} \right|, \quad (6)$$

where we have normalized the flux density by the maximum magnetic flux density  $\langle B_0 \rangle$  that can be generated through the antenna. This field occurs when the antenna current is  $I_0 = V_s (4R_0 R_A)^{-1/2}$ , i.e., the maximum amount of power from the amplifier is dissipated across the resistor  $R_A$  that is in series with the antenna inductor.

With Eq. (6) we have a metric—analogue to the transducer power gain<sup>16</sup> employed for power matching systems—that represents the relative performance of the tuning network in generating a magnetic flux density from a single source. We use this equation to guide the design of VDWLs specific to the various applications discussed in the previous section. This is particularly important for choosing circuit components in Fig. 1 since these will depend on the frequency range and de-

sired power levels of the application as well as the non-ideal behavior of the circuit elements. In order to illustrate a procedure for selecting the appropriate components for an application, we discuss in the next section an illustrative example with an actual VDWL. We also use Eq. (6) to demonstrate the efficacy of the system in achieving (I) and (II), the goals stated in the previous section.

### III. VDWL FOR THE BEATING WAVES EXPERIMENT II

In this section, we present the VDWL for the beating waves experiment II (BW X II). The primary goal of this setup is to investigate experimentally the non-linear heating that can arise when the so-called beating criterion<sup>2,4</sup> is satisfied:  $f_2 - f_1 = n f_{ci}$ . As the level of heating depends on this condition as well as the individual wave frequencies  $f_1$  and  $f_2$ , this system is a well-suited application for the VDWL outlined in Sec. II. In the following discussion, we describe the experimental setup of BW X II, present the antenna and matching components employed in its VDWL, and outline the plasma modes we expect to propagate in the BW X II plasma.

#### A. Experimental setup

The experimental setup for BW X II (Ref. 17) is shown in Fig. 2. It consists of an axially symmetric, uniformly magnetized argon plasma sustained by an inductive, radio frequency discharge. The vacuum chamber is a pyrex cylinder 132 cm in length with a 16.5 cm inner diameter placed concentrically in a 122 cm long, 10 ring solenoid. This configuration provides a uniform magnetic field of  $750 \pm 5$  G ( $f_{ci} \approx 27.5$  kHz) in the axial direction over the length of the heating antenna, which accommodates a frequency range of interest of  $f_1 = f_{ci} - 5.5 f_{ci} \approx 27.5 - 150$  kHz. A constant pressure of 0.1 to 10 mTorr is maintained by a 140 l/s turbo pump with conductance controller in tandem with a roughing pump.

The plasma discharge is provided by a Boswell-type saddle antenna<sup>18,19</sup> with a 18.4 cm inner diameter placed around the vacuum chamber at one end of the solenoid. The antenna is powered by a 1.25 kW source operated at 13.56 MHz and matched to the plasma with an L network consisting of two Jennings 1000 pF variable vacuum capacitors. Once generated, the argon plasma propagates along the magnetic

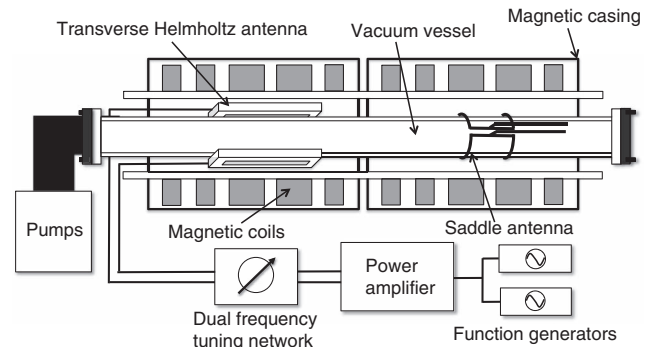


FIG. 2. Diagram of the beating waves experiment II.



field lines to the central part of the experiment where the plasma heating occurs.

The plasma heating is produced by the non-linear interaction of the plasma with two, perpendicularly propagating electrostatic waves. The combined signal of two Wavetek 180 signal generators provides the source waveform for these waves, which is amplified by an ENI 2100L broadband amplifier with a  $50\ \Omega$  source impedance.

### 1. Inductive antenna

In BWX II, we employ a Helmholtz antenna to couple to electrostatic ion cyclotron modes in the plasma. It consists of two  $24.1\ \text{cm} \times 16.5\ \text{cm}$  rectangular coils that cover a cross-section of the plasma with the longer dimension along the axis of the plasma. For a given current, this configuration concentrates the magnetic flux density directly in the volume where electrostatic waves are desired. Each coil is wound with twenty turns of 14 AWG copper wire that are spaced in order to minimize parasitic capacitance between windings as well as resistive losses that arise from proximity effects.<sup>20</sup> The real and imaginary components of the impedance of the antenna were measured directly at the leads by comparing the magnitude and phase of a sinusoidal signal from the ENI2100L at the indicated frequency. These measurements were verified with a low-frequency dual directional coupler. The results are shown in Fig. 3 for the case of an input power of 50 W.

The self-resonant frequency of the antenna that results from parasitic capacitance between the windings and the environment of BWX II occurs at 1.1 MHz. This leads to an equivalent circuit model (Fig. 1) for the antenna where a small capacitance,  $C_A = 66\ \text{pF}$  is in parallel with an inductor  $L_A = 317\ \mu\text{H}$  and resistor  $R_A$  in series. The calculated series resistance,  $R_A$ , which is shown in Fig. 3, increases by a factor of four over our frequency range due to AC resistive losses.

### 2. Variable capacitors

Each LC trap of the circuit employs a 1–1000 pF vacuum variable Jennings capacitor. We used a set of fixed elements

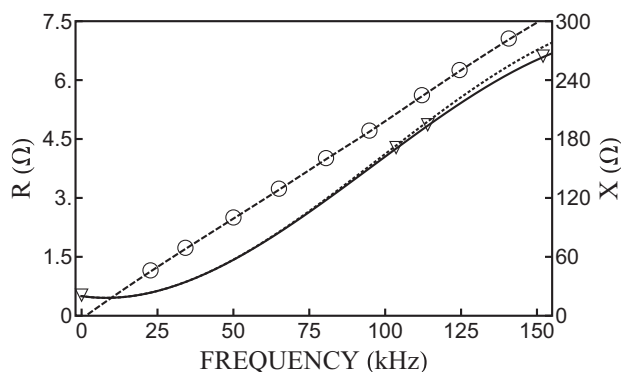


FIG. 3. The measured impedance of antenna with an interpolation fit. The dashed line corresponds to the reactance and the solid is the overall resistance. The dotted line is the calculated value of the resistor,  $R_A$ , for an equivalent circuit model of the antenna that is comprised of the series resistor and inductor ( $L_A = 317\ \mu\text{H}$ ) in parallel with a capacitor ( $C_A = 66\ \text{pF}$ ). These impedance measurements were taken for an input power of 50 W.

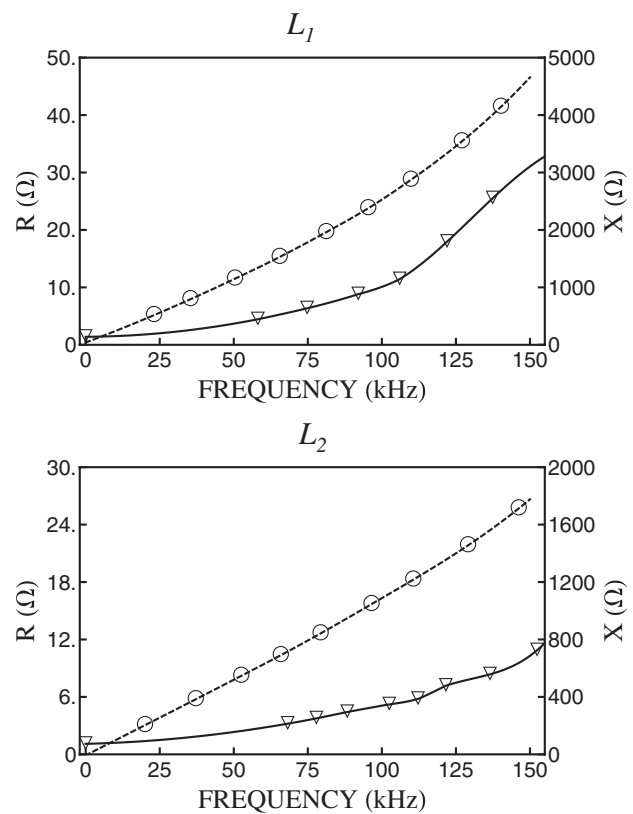


FIG. 4. Impedance of the two air-core inductors employed in the matching network for an input power of 50 W. The solid line ( $\nabla$ ) corresponds to the real component of the impedance while the dotted ( $\circ$ ) represent the reactive component.  $L_1 = 3.7\ \text{mH}$  and  $L_2 = 1.7\ \text{mH}$ .

(four 1000 pF Mica capacitors and one 10 000 pF Mica capacitor) placed in parallel with the vacuum variable capacitors in order to yield a variable range of capacitance of  $C_1$  from 1–10 000 pF and  $C_2$  from 1–5000 pF. In general, we have found the parasitic inductance and resistance of the capacitors are small when compared to the parasitic elements of the inductors. This verifies our depiction in Fig. 1 of  $C_1$ ,  $C_2$  as ideal elements.

### 3. Inductors

We chose to use air-core, cylindrical inductors in order to avoid core losses<sup>21</sup> at the high inductances and powers required for BWX II. The disadvantage of this configuration is that a large number of turns are required, which can lead to large parasitic interwinding capacitance, AC series resistance, and stray capacitances. We minimized these effects by isolating the inductors from the surrounding environment and winding them in single layers with length to diameter ratios of approximately one.<sup>22</sup> In this way, we constructed two inductors from 14 AWG copper wire that measured 35.6 cm and 26.7 cm in diameter with inductances of  $L_1 = 3.7\ \text{mH}$  and  $L_2 = 1.7\ \text{mH}$ . The measured impedances for these inductors are shown in Fig. 4 for an input power of 50 W. From these measurements, the parasitic capacitances were found to be  $C_{p1} = 90\ \text{pF}$  and  $C_{p2} = 110\ \text{pF}$ . As with the case of the Helmholtz antenna, the values of  $R_{p1}$ ,  $R_{p2}$  increased over

the frequency range due to AC resistive effects. However, since the calculation of  $\beta$  in Eq. (6) only requires an estimate for the total impedance  $Z_T$ , instead of determining the explicit frequency dependencies of the equivalent circuit elements  $R_{p1}$ ,  $R_{p2}$ , we used interpolation fits to the total measured impedances of each inductor in our calculations for the normalized flux density.

#### 4. Transformer

For the BWX II application, we employ a 2:1 ( $n = 2$ ) current transformer to provide an approximate match of the combined resistance from the non-ideal inductors and antenna to the  $50 \Omega$  source impedance over the frequency range. Conventional power transformers, which employ ferrite or iron cores, are plagued by the same saturation effects and core losses in BWX II as the aforementioned inductors. This is a consequence of the the core's primary role in transferring energy between primary and secondary windings. An air core transformer avoids saturation; however, the loss in magnetic coupling that results from the absent core significantly reduces the transformer's performance. Given these inherent difficulties with the conventional configuration, we instead chose to employ a Ruthroff transmission line transformer<sup>23</sup> that consisted of several windings of  $50 \Omega$  coaxial cable around a toroidal magnetic core of type W-material. The advantage of this method is that instead of transferring energy, the core serves as a choke to prevent current imbalance between the center conductor and shield. We have found that the core performance is close to ideal over our ultrasonic frequency range when connected to effective resistive loads on both ends. It is for this reason that this type of transformer works particularly well with the VDWL shown in Fig. 1 as it is placed between the resistive source and a conjugately matched load at the frequencies of interest.

#### B. Excited modes in BWX II

The coupling of the VDWL to plasma modes in BWX II depends on the magnitude of the magnetic flux density generated in the volume. However, while the VDWL serves to maximize this flux density over the range of frequencies of interest, the plasma parameters, antenna geometry, and background magnetic field all dictate the accessibility and types of plasma modes induced in the plasma.

With this in mind, since the goal of BWX II is to investigate the heating produced by the non-linear interaction of *perpendicularly*-propagating electrostatic waves, the aspect ratio of the antenna was made deliberately small ( $< 1$ ). This results in induced charge gradients that couple primarily to *perpendicularly*-propagating modes where the components of the wavenumbers satisfy  $k_{\perp} \gg k_{\parallel}$ .

In order to minimize noise from the 13.56 MHz RF source and to ensure a flatter radial density profile, the BWX II was operated in the inductive mode at the moderate RF discharge power of 300 W with a background pressure of 1 mT. The electron temperature, which was measured with an array of double langmuir probes, was found to be approxi-

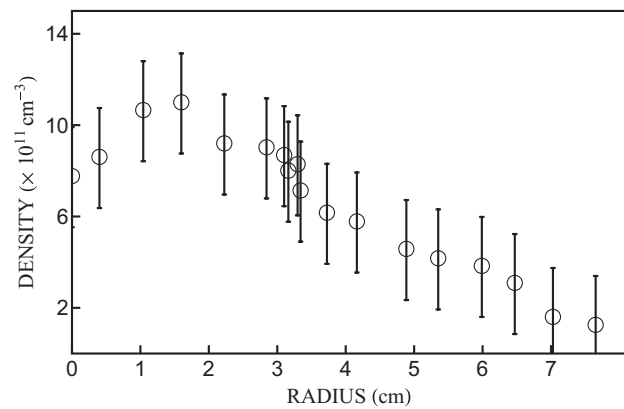


FIG. 5. Characteristic radial profile for density in the BWX II heating volume taken at the axial center of the Helmholtz antenna.

mately uniform over the majority of the heating volume with  $T_e \approx 3.5$  eV. We observed a small increase in temperature at the plasma edge, which is consistent with cylindrical inductively coupled sources.<sup>24</sup>

A typical density profile for the operating conditions of BWX II is shown in Fig. 5. As can be seen, there is an approximately uniform region of density near the center of the plasma with a small dip at  $r = 0$ . This same trend has been reported for similar inductive discharges at low power.<sup>25</sup> The axial dependence of both temperature and density was found to be uniform for the length of the heating volume, i.e. the axial extent of the Helmholtz antenna. The ion temperature, which was measured with a laser induced fluorescence system, was approximately 0.1 eV.

Since the axial length of the antenna (24.1 cm) necessarily dictates that  $k_{\parallel} < 0.26 \text{ cm}^{-1}$ , we see that in the region near the center of the plasma, the parallel phase velocity is constrained over the frequency range of interest such that  $(2\kappa T_i/m_i)^{1/2} < \omega/k_{\parallel} < (2\kappa T_e/m_e)^{1/2}$  and  $\omega_{ci} < \omega_{pi}$  where  $\omega_{pi}$  denotes the ion plasma frequency,  $m_e$ ,  $m_i$  are the species masses,  $\kappa$  is the Boltzmann constant, and  $\omega = 2\pi f$  is the angular frequency of the wave. Furthermore, as the density variation for the region near the center of the plasma is small, we make the approximation that the plasma is homogenous and isotropic in this area. Under this assumption, it has been demonstrated analytically that for waves with phase velocities constrained by the above conditions, it is possible for two electrostatic modes to propagate in a magnetized plasma—the large wavelength, small electrostatic ion cyclotron wave (EICW) and the small wavelength, backward-propagating neutralized ion Bernstein wave (NIBW).<sup>10,26</sup> However, given the low ionization fraction in the plasma, we anticipate that the smaller wavelength NIBW branch will be subject to significant collisional damping.<sup>27</sup> Therefore, the EICW should be the dominant mode in the plasma. The dispersion relation for this wave under the assumption of cold-ions and isothermal electrons is given by

$$\omega^2 = \omega_{ci}^2 + \frac{\kappa T_e}{m_i} k_{\perp}^2. \quad (7)$$

This dispersion relation exhibits a cut-off at the ion cyclotron frequency such that modes excited below this frequency will

evanesce. For waves with frequencies exceeding this cut-off condition,  $\omega > \omega_{ci}$ , we anticipate EICW waves to propagate near the center of the plasma.

We further anticipate that these modes should be able to propagate across the density gradient from the plasma boundary to the region of uniform density. Indeed, it has been shown that a drop in density at the plasma edge can help facilitate coupling to electrostatic modes that have non-zero (though small) components of  $k_{\parallel}$ .<sup>28,29</sup>

### C. Results

For experiments with the VDWL in BWX II, it was found that the plasma loading was small:  $R_p < 0.5\Omega$ ,  $L_p \ll L_A$  where  $R_p$ ,  $L_p$  denote the plasma resistance and inductance respectively. Therefore the matching conditions were primarily dictated by the impedance of the inductive antenna. In the first section, we neglect plasma loading in evaluating the ability of the VDWL to maximize magnetic flux density in the heating volume. We complement this discussion then with direct measurements of propagating modes in the plasma that provide evidence for the VDWL's ability to couple waves into the BWX II plasma.

#### 1. Antenna flux density

Ignoring the small effects of plasma loading, we now examine the normalized flux density in our antenna as a function of wave frequency and capacitance by numerically evaluating Eq. (6) with the measured impedances of our components reported in the previous section. In order to illustrate the parameters we will investigate, we show in Fig. 6 a sample plot of the normalized magnetic flux density produced by the BWX II antenna in the heating region as a function of frequency for fixed capacitor values of  $C_1 = 1640$  pF and  $C_2 = 1770$  pF. This figure shows two peaks at the frequencies  $f_1$  (60 kHz) and  $f_2$  (85 kHz) with values of  $\beta_1$  (0.57) and  $\beta_2$  (0.6). The full-width half maximum (FWHM) of each peak is denoted as  $w_1$  (1.5 kHz) and  $w_2$  (1.5 kHz) respectively. It is evident from

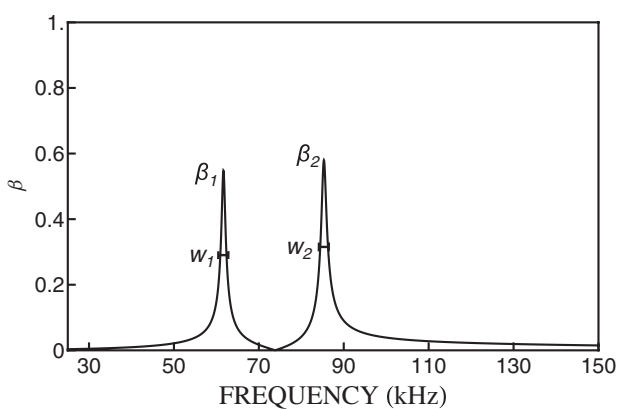


FIG. 6. The normalized, magnetic flux density for the wave launching system as a function of frequency. The peaks occur at frequencies  $f_1$  (60 kHz),  $f_2$  (85 kHz);  $\beta_1$  (0.57),  $\beta_2$  (0.6) correspond to the values of the normalized flux density at the peaks; and  $w_1$  (1.5 kHz),  $w_2$  (1.5 kHz) are the FWHMs.  $C_1 = 1640$  pF,  $C_2 = 1770$  pF.

this figure that the network is capable of producing magnetic flux densities at over 50% of the ideal case at two frequencies simultaneously. Moreover, the small width of each peak indicates that the network effectively attenuates the surrounding spectrum.

In order to gauge the success of the VDWL over the entire frequency spectrum, we devised a procedure to find a single term that could reflect the average tuning capability of the network. To this end, we fixed  $f_1$  and  $f_2$  in the frequency range and numerically determined from Eq. (6) the capacitor values that yielded the highest average value of the two peaks  $\beta_1$ ,  $\beta_2$ . We denote this as  $\beta^*(f_1, f_2) = [(\beta_1(C_1, C_2) + \beta_2(C_1, C_2))/2]_{\max|f_1, f_2}$  where  $f_1$ ,  $f_2$  are constant and  $C_1$ ,  $C_2$  are the variables used to maximize the term. We then held  $f_1$  constant and repeated this procedure for incremented values of  $f_2$  in the frequency range. With this data set, we averaged over  $f_2$  to yield  $\bar{\beta}(f_1) = \langle \beta^*(f_1, f_2) \rangle_{f_2}$  as a function of  $f_1$ . The process was then iterated for a new value of  $f_1$  in order to arrive at the plot shown in Fig. 7(a). Typical error bars are also shown.

Each point in this figure represents the average peak value that can be achieved when  $f_1$  is fixed and  $f_2$  is allowed to vary

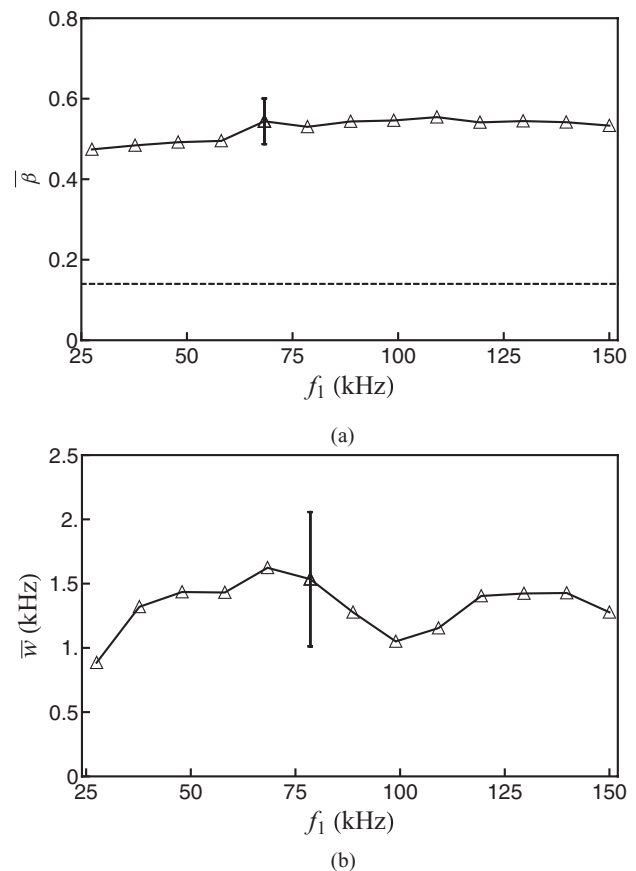


FIG. 7. (a) Each point is the average of the maximum, normalized magnetic flux density achieved simultaneously by the network at fixed frequency  $f_1$  and frequency  $f_2$  where the average is performed over  $27.5 < f_2 < 150$  kHz. The dotted line corresponds to the maximum flux density for the antenna without a matching network. (b) Values are the average of the FWHM of the optimized dual peaks that occur at the fixed frequency  $f_1$  and frequency  $f_2$  where the averaging is the same as in (a). In both cases, the averaging is performed such that  $|f_2 - f_1| > 10$  kHz.

over  $27.5 < f_2 < 150$  kHz. The figure is therefore an indication of the overall tuning capability of the network for almost all combinations of frequencies. There is one significant exception to this generalization: in our iteration procedure, all of our frequencies were chosen such that  $|f_2 - f_1| > 10$  kHz. This is a restriction specific to BWX II, as in this experiment we investigate waves whose frequencies differ by values larger than the cyclotron frequency (27.5 kHz). When  $f_1 \rightarrow f_2$ , however, the ability of the network to isolate peaks is drastically reduced. This would skew the results in Fig. 7(a) to values lower than would be achieved for our application. With this in mind, we see from this plot that provided  $|f_2 - f_1| > 10$  kHz, we generally can tune the network such that the magnetic flux density generated at each desired frequency is greater than 50% of ideal. By comparison, we also show in Fig. 7(a) the dotted line that corresponds to the maximum normalized magnetic field that can be generated in the antenna without a tuning network or transformer. It is evident from this plot that the VDWL produces significantly improved results over the unmatched case.

In order to quantify the ability of the network to isolate dual, variable frequencies while attenuating the rest of the spectrum, we followed the same averaging procedure outlined above to determine  $\bar{w}(f_1)$  for the optimized values of  $\bar{\beta}$ . This is shown in Fig. 7(b) where we see the average FWHM of each peak ( $< 2$  kHz) corresponds to  $|f_2 - f_1|/f_{ci} < 10\%$  for the BWX II experimental parameters. This excellent attenuation suits the careful tuning of frequencies required for the BWX II two-wave investigation. Moreover, this performance offers a vast improvement over the unmatched case where all frequencies are passed ( $w_1, w_2$  are unbounded).

As an additional evaluation of this network, we consider the necessary capacitances to achieve the desired matched frequencies. Using the values of  $C_1, C_2$  that optimized  $\beta^*(f_1, f_2)$ , we have plotted as markers in Fig. 8 the average values of  $C_1$  that produced  $\beta_1$  at  $f_1$  and the average values of  $C_2$  that yielded  $\beta_2$  at  $f_2$ . We also have included as dotted lines the ideal relations as given by Eq. (5). There is good agreement at the extremes of the frequency region where the larger inductor and capacitor series ( $L_1, C_1$ ) follows the asymptotically derived equation for the low end of the spectrum and the smaller inductor-capacitor series ( $L_2, C_2$ ) is successfully modeled for high frequencies. Equation (5) thus serves as a reliable, first indicator of the range of capacitance to which we must tune in order to achieve the highest  $\bar{\beta}$ , and any deviations can be accounted for by using the data plots shown in Fig. 8. More importantly, we see that the matching conditions do not call for capacitances outside of our variable tuning range.

## 2. Evidence for wave propagation

While Sec. III C 1 illustrated the ability of the VDWL to maximize magnetic flux density in the heating volume over the desired frequency range of BWX II, in order to verify that this flux density successfully excited propagating electrostatic waves, we measured coherent fluctuations in the plasma density with an axially-translated array of positively biased, single-tip langmuir probes over a  $5 \text{ cm} \times 5 \text{ cm}$  cross-sectional area in the plasma. Measurements were performed

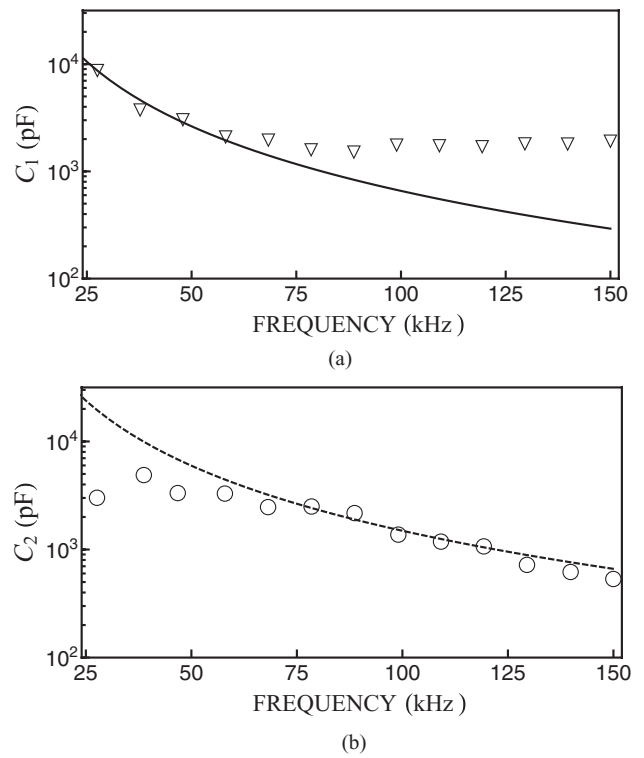


FIG. 8. (a) The average capacitance of  $C_1$  ( $\nabla$ ) that yields the optimized magnetic flux density at fixed  $f_1$  and  $f_2$  where an average is taken over all values of  $f_2$  in the spectrum. (b) The average capacitance of  $C_2$  ( $\circ$ ) that yields the optimized magnetic flux density at fixed  $f_1$  and  $f_2$  where the average is performed over all values of  $f_1$  in the spectrum. In both cases, the averaging is performed such that  $|f_2 - f_1| > 10$  kHz. The dotted line in each figure corresponds to the ideal tuning conditions represented by Eq. (5).

both for the case of a single frequency  $f_1$  and two frequencies,  $f_1, f_2$  excited simultaneously. The signal to noise ratio of these measurements was increased with a Stanford SR830 lock-in amplifier that was referenced with the input signal of the frequency of interest. This lock-in amplifier served the additional purposes of isolating signals when two frequencies were excited simultaneously. The frequency range of the lock-in amplifier for these measurements ranged from 1 Hz–100 kHz, which placed an upperbound on the measurements of the wave fluctuations.

For RF input powers of 100 W, we consistently found coherent density functions  $\delta n_e/n_e$  from 5–20% over the investigated frequency range of  $20 \text{ kHz} < f_1, f_2 < 100 \text{ kHz}$ . Using a standard probe interferometry technique,<sup>10,12,30</sup> we further found that these fluctuations propagated in the plasma with finite wave numbers. This confirmed that the modes were not simply the product of electric pick-up at the probe tips.<sup>31</sup>

In order to identify the modes propagating in the plasma, we Fourier analyzed a series of spatial interferometry scans for the case of a single wave  $f_1$ . This revealed that the parallel wave number exceeded the length of the scanning such that  $k_{\parallel} < 0.26 \text{ cm}^{-1}$  and that the perpendicular wavenumbers satisfied the EICW dispersion. A series of sample data points from the scan and the ideal dispersion relation are shown in Fig. 9. The solid line is a best fit parameter which corresponds to Eq. (7) for an electron temperature of  $T_e = 3.4 \text{ eV}$ . This close proximity to the value of  $T_e = 3.5 \text{ eV}$  measured with



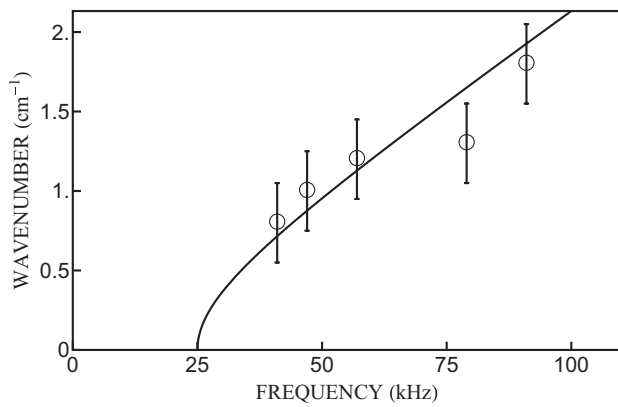


FIG. 9. Measured wavenumber as a function of frequency in BWX II for a single wave excited with the Helmholtz antenna. The solid line is the ideal dispersion relation for an EICW with an electron temperature of  $T_e = 3.4$  eV.

the double probe array also corroborates the EICW nature of these excited modes.

As a final consideration, we investigated the dependence of wave amplitude on the power in the heating antenna. It has been reported in previous electrostatic wave experiments that for increasing power levels of waves excited by external sources, non-linear effects can lead to saturation in the wave amplitude.<sup>32</sup> We did not see this effect, however, even at the maximum 200 W power output of the ENI 2100L. Rather, the wave amplitude was observed to increase with power until the upperbound in amplifier power was reached.

#### IV. DISCUSSION

The results from the previous section serve to validate our VDWL by demonstrating the system's ability to achieve the exacting tuning goals (I and II) of the BWX II investigation and to successfully couple to propagating modes in a plasma. At the same time, this illustrative example also provides us with insight for how the VDWL concept may be tailored to applications that call for larger magnetic flux densities, higher powers, and different frequency ranges.

For applications such as atmospheric studies that require tuning features similar to the BWX II VDWL but higher magnetic flux densities in order to couple waves into a less dense plasma, it is necessary to address the non-idealities in the matching components encountered in BWX II. While the BWX II system clearly outperforms an unmatched antenna, we have found that the maximum achievable  $\bar{\beta}$  of the network is bounded both by the AC resistances in the inductors and the increasing resistance of the antenna with frequency. These effects may be mitigated in part by using windings designed to minimize AC resistance such as Litz wire; however, this must be done with care as the close proximity of windings in this configuration has the deleterious effect of increasing parasitic capacitances.

As a second consideration, the VDWL for BWX II has been designed and tested for powers up to 200 W, which corresponds to antenna currents on the order of 10 A. Industrial and plasma heating applications that call for higher power levels can employ a similar VDWL as the one designed for BWX

II, but it will be necessary to take steps to reduce the voltage drop across the capacitors to avoid breakdown. This is most important when small capacitance is required (at the upper-bound of the frequency range) as the voltage drop across the inductor scales inversely with capacitance. In order to achieve these small values at high voltages, it will be necessary either to employ more robust components or place the padding capacitors in series with the variable capacitors. At these higher power levels, amplitude saturation of the coupled modes in the plasma may also be a concern.

Finally, from BWX II's example, we see that it is possible to adapt the VDWL with relative ease to applications with different frequency ranges and antennae with different geometries. The procedure for this adaptation follows the same outline as above: measure the impedance of the antenna, follow the criterion that  $L_1, L_2 \gg L_A$ , use these selected inductor values along with the desired frequency range to determine the necessary range of capacitance from Eq. (5), measure the actual impedance of each component over the frequency range in order to find  $Z_T$  and  $Z_A$ , and use Eq. (6) to estimate the normalized magnetic field generated as a function of frequency. The robustness and predictability of the network can be gauged using plots similar to those presented in Figs. 7 and 8.

#### V. CONCLUSION

We have presented a dual-frequency, variable wave launching system that is capable of selectively passing two frequencies concurrently from a single amplifier. We outlined the two essential components for the system, the loop antenna and matching network, and derived the equations necessary for gauging the efficacy and robustness of this system. We further provided an example of a successful VDWL employed in a scientific application, the beating waves experiment II, and discussed a procedure for how the VDWL can be adapted to a number of different uses. From these considerations, we see that the VDWL permits the necessary measure of control for applications that depend on the excitation of two electrostatic waves.

#### ACKNOWLEDGMENTS

The authors would like to acknowledge Nevell Greenough and Elmer Fredd of the Princeton Plasma Physics Laboratory for their assistance in procuring components for the tuning network. This material is based upon work supported by the National Science Foundation Graduate Research Fellowship under Grant No. 0646086.

<sup>1</sup>A. Ram, A. Bers, and D. Benisti, *J. Geophys. Res.* **103**, 9431, doi:10.1029/97JA03668 (1998).

<sup>2</sup>D. Benisti, A. K. Ram, and A. Bers, *Phys. Plasmas* **5**, 3224 (1998).

<sup>3</sup>D. Benisti, A. K. Ram, and A. Bers, *Phys. Plasmas* **5**, 3233 (1998).

<sup>4</sup>R. Spektor and E. Y. Choueiri, *Phys. Rev. E* **69**, 046402 (2004).

<sup>5</sup>Z.-M. Sheng, L. Yu, G. Hao, and R. White, *Phys. Plasmas* **16** (2009).

<sup>6</sup>B. Jorns and E. Y. Choueiri, *Phys. Rev. Lett.* **106**, 085002 (2011).

<sup>7</sup>B. Jorns and E. Choueiri, in *46th Joint Propulsion Conference and Exhibit, Nashville, TN, AIAA-2010-7107* (2010).

<sup>8</sup>W. M. Hooke and S. Bernabei, *Phys. Rev. Lett.* **28**, 407 (1972).

<sup>9</sup>A. Fasoli, F. Skiff, R. Kleiber, M. Q. Tran, and P. J. Paris, *Phys. Rev. Lett.* **70**, 303 (1993).

- <sup>10</sup>J. Goree, M. Ono, and K. Wong, *Phys. Fluids* **28**, 2845 (1985).
- <sup>11</sup>F. Skiff, F. Anderegg, and M. Q. Tran, *Phys. Rev. Lett* **58**, 1430 (1987).
- <sup>12</sup>J. Schmitt, *Phys. Rev. Lett.* **31**, 982 (1973).
- <sup>13</sup>R. L. Stenzel and W. Gekelman, *Phys. Rev. A* **11**, 2057 (1975).
- <sup>14</sup>M. Light and F. Chen, *Phys. Plasmas* **2**, 1084 (1995).
- <sup>15</sup>J. L. Kline, E. E. Scime, P. A. Keiter, M. M. Balkey, and R. F. Boivin, *Phys. Plasmas* **6**, 4767 (1999).
- <sup>16</sup>B. Yarman, *Design of Ultra Wideband Power Transfer Networks* (Wiley, Chichester, West Sussex, UK, 2010).
- <sup>17</sup>B. Jorns and E. Choueiri, in *45th Joint Propulsion Conference and Exhibit, Denver, CO*, AIAA-2009-5367 (2009).
- <sup>18</sup>R. W. Boswell, *Physics Letters A* **33**, 457 (1970).
- <sup>19</sup>R. W. Boswell, *Plasma Phys. Controlled Fusion* **26**, 1147 (1984).
- <sup>20</sup>A. Urling, V. Niemela, G. Skutt, and T. Wilson, in *Applied Power Electronics Conference and Exposition* (1989), pp. 373–385.
- <sup>21</sup>W. Mclyman, *Transformer and Inductor Design Book* (Marcel Dekker, New York, NY, 2004).
- <sup>22</sup>F. Terman, *Electronic and Radio Engineering* (McGraw-Hill, New York, NY, 1955).
- <sup>23</sup>J. Sevick, *Transmission Line Transformers*, 4th ed. (Noble, Atlanta, GA, 2001).
- <sup>24</sup>F. Chen and J. Chang, *Lecture Notes on Principles of Plasma Processing* (Kluwer Academic/Plenum, New York, 2003).
- <sup>25</sup>M. A. Lieberman and R. W. Boswell, *J. Phys. IV France* **08**, Pr7 (1998).
- <sup>26</sup>T. Stix, *Waves in Plasmas* (American Institute of Physics, New York, 1992).
- <sup>27</sup>R. Spektor, *Ion Acceleration by Beating Electrostatic Waves*, Ph.D. dissertation, Princeton University, 2006.
- <sup>28</sup>W.-C. Sy, T. Amano, R. Ando, A. Fukuyama, and T. Watari, *Nucl. Fusion* **25**, 795 (1985).
- <sup>29</sup>M. Brambilla, *Nucl. Fusion* **28**, 549 (1988).
- <sup>30</sup>R. P. H. Chang and M. Porkolab, *Phys. Fluids* **13**, 2766 (1970).
- <sup>31</sup>*Methods of Experimental Physics*, edited by H. Griem and R. Lovberg (Academic Press, New York, 1970), Vol. 9.
- <sup>32</sup>A. Fasoli, F. Skiff, and M. Q. Tran, *Phys. Plasmas* **1**, 1452 (1994).